Evidence of absorption dominating over scattering in light attenuation by nanodiamonds

S. V. Koniakhin,[1, 2, 3, ∗] M. K. Rabchinskii,[2] N. A. Besedina,[2, 3]

L. V. Sharonova,[2] A. V. Shvidchenko,[2] and E. D. Eidelman[2, 4]

[1]*Institut Pascal, PHOTON-N2, University Clermont Auvergne,
CNRS, 4 avenue Blaise Pascal, 63178 Aubière Cedex, France*
[2]*Ioffe Institute, 194021 St. Petersburg, Russia*
[3]*St. Petersburg Academic University - Nanotechnology Research and Education
Centre of the Russian Academy of Sciences, 194021 St. Petersburg, Russia*
[4]*St. Petersburg Chemical Pharmaceutical Academy, 197022 St. Petersburg, Russia*

We show an experimental evidence of the domination of absorption over scattering in absorbance spectra of detonation nanodiamond hydrosols. We perform the absorbance measurements on the UV-vis spectrophotometer equipped with integrating sphere and compare them with conventional absorbance spectra. Additionally, we measure the scattering light intensity at the cuvette side wall (scattering at 90 degrees angle). The obtained experimental data were interpreted using the photon random walk simulations based on the scattering cross sections and indicatrices given by the Mie theory.

We conclude that the scattering is governed only by the agglomerates $\gtrsim$ 100 nm, remaining in the hydrosols, and their fraction can be effectively controlled by centrifugation. For the primary 4 nm crystallites, the light extinction is due to absorption only and scattering can be neglected. Another important result is that the Mie theory is obligatory for the description of the nanodiamond hydrosols optical properties due to the interplay between the size, fractal dimension, and dielectric properties of the agglomerates. Finally, based on the obtained absorption spectra the fraction of non diamond phase in the diamond nanoparticles was estimated.

I. INTRODUCTION

Nanodiamonds are one of the most unique nanoparticles being currently investigated due to their exceptional mechanical, heat and optical properties inherited from the bulk diamond[1–5]. Nanodiamonds exhibit high thermal conductivity[6] and mechanical strength, can contain bright, long-lived and controllable color centers[7–11]. Current and future applications of nanodiamonds include NV defects-based quantum computing[12–14], composite materials creation[6,15–17], bioimaging[18,19], and drug delivery[20]. Along with manufacturing, modifying, and investigating the high-pressure high-temperature[19,21,22], bead milling[7], laser synthesis[23], and even extraterrestrial[24] nanodiamonds, among the most promising are the detonation nanodiamonds (DND)[4,25]. Besides the powders, the most important form for DND and other nanodiamonds are the water suspensions (hydrosols), easy-to-handle and native for chemistry and biology. Despite the serious progress that was achieved in the nanodiamond size control and fractionation[22,26,27], the hydrosols contain both individual primary crystallites and their agglomerates. Moreover, individual DND particles tend to form chains in hydrosols[28].

To better understand the size distribution, structure, and phase composition of nanodiamonds, the optical experiments including measuring Absorbance (Abs) spectra are widely used[29–33]. One of the most conventional and widely applied methods of nanodiamond characterization is dynamic light scattering (DLS)[34–37], which requires precise knowledge of the optical parameters of the materials. This makes the deeper understanding of nanodiamond hydrosols optical properties highly desired. The surface effects closely connected with optical absorption are important for the manifestation of NV defects and for the quenching of their luminescence[38–40].

Abs spectra (also referred as UV-vis spectra or Optical density spectra) of detonation nanodiamond hydrosols can be described as a superposition of light scattering and absorption[30,31]. The peculiar shape of the optical density spectra is thought to be defined by the interplay between these two effects, with the domination of scattering. For calculating the scattering cross section, the Rayleigh and Mie theories are used. Calculating the absorption cross section requires a model where nanoparticle electric polarization contains the imaginary part. Usually, the nanoparticle core-shell models with the presence of diamond-like core and graphite-like phase on the surface[29,30,41] are used, where the dielectric constant of graphite-like phase contains significant imaginary part giving the absorption. Numerical values of graphite-like dielectric constant are approximated with data for bulk graphite[42]. The calculations predict that the scattering dominates the absorption by a factor of 10 at shorter wavelengths (lower than 500 nm), whereas in red and near-IR regions the contribution of scattering and absorption becomes comparable[30].

Another approach for the determination of nanodiamond optical properties is based on ab-initio calculation of the nanodiamond electronic structure and derivation of the corresponding light absorption[43]. These calculations allow accounting for such effects as surface reconstruction, presence of amorphous phase and carbon atoms with intermediate between sp^2 and sp^3 hybridization.

Here, we present an experimental evidence that 4 nm nanodiamonds dominantly *absorb* light in all visible range, including near-UV and near-IR, which differs from the previous models suggesting that Abs spectra of DND hydrosols are mainly governed by the scattering. This picture generally remains valid even for agglomerates, where the absorption is determined to be comparable with the scattering. These results lead to a global change of the paradigm of the DND hydrosols Abs spectra interpretation.

The paper is organized as follows. In section II A, we describe the preparation of the samples. The main quantity about which the present paper is composed is light intensity I_{sca}, scattered by nanodiamonds in the hydrosol and thus gone away from the cuvette. At a qualitative level, it is obvious that I_{sca} positively correlates with the scattering cross section of the nanoparticles in hydrosol and negatively correlates with the absorption cross section. I_{sca} can be addressed in three ways:

- Calculated via the difference between the Abs spectra measured with integrating sphere (IS) and without it (section II B).

- Detected straightly as the light intensity scattered at 90 degree angle through the cuvette side wall (section II C).

- Via the numerical simulation of the photon random walks in the medium where scattering and absorption takes place (section III).

In section IV we describe the obtained experimental and theoretical results and in section V we discuss them and establish a relation between all three approaches mentioned above. We will show that from the experimental results one can quantitatively conclude on the absorption and scattering contributions. The comparison of the experimental data and results of the simulation provides the quantitative level of extracting contributions to DND absorbance from scattering and absorption.

II. EXPERIMENT

A. Samples

As an initial DND, the powder of an industrial DND was taken and an additional purification with the mixture of HF and HBr from inorganic impurities was done to obtain Z0 sample. DND Z0 powder was annealed in hydrogen at 600° C for 3 hours for producing DND Z+ sample. DND Z- was obtained after annealing Z0 powder in air at 450° C for 6 hours. These protocols follow the procedures described in Ref.[27]. Thus, three DND powders (Z0, Z+, and Z-) were obtained. The difference in deagglomeration procedure leads to a difference in surface chemistry of the samples. DND Z- and Z+ are both grafted with CH and -COOH/-C(O)O- groups, however

in different relations. DND Z- surface contains mainly carboxyls and lactones[44], while Z+ is hydrogenated.

The additional fractionation of the hydrosols was performed as follows. All three powders were dispersed in demineralized (deionized) water by ultrasonic treatment. The initial concentration of nanodiamond in water was ca. 1 wt. %. After dispergation, the resulting hydrosols were centrifuged at 18000g for 40 minutes (Sigma 3-30KS centrifuge). In each capsule for centrifugation, a hydrosol has a volume of approx. 6 ml. Thus, primary 4 nm crystallites that did not settle during the centrifugation process and larger particles (agglomerates) were separated. The supernatants recovered after centrifugation are referred as DND Z01 (0.08 wt%), Z+1 (0.44 wt%) and Z-1 (0.35 wt%) hydrosols. The precipitates diluted with demineralized water and ultrasonically treated are DND Z02 (0.58% by weight), Z+2 (1.07% by weight) and Z-2 (1.28% by weight). Their concentrations (WT1) were measured by drying 10 g of each hydrosol, followed by measuring the mass of the sediment on an analytical scale SartoGosm CE-124C. Finally, the additional dilution of the hydrosols was done to achieve the abosrbance values of 0.3, most suitable for optical measurements due to lowering the effects of multiple scattering and reabsorption. The weight fractions after dilution are designated as WT2. The corresponding data is listed in Table I. Size distributions were obtained using the Malvern ZetaSizer device.

TABLE I. Weight fractions of nanodiamonds in hydrosols. WT1 - after centrifugation. WT2 - after dilution and before optical measurements. The concentrations of primary particles n_P and agglomerates n_1 and n_2 obtained from the simulations described below are also given.

Sample	WT1, %	WT2, %	n_P, cm^{-3}	n_1, cm^{-3}	n_2, cm^{-3}
Z+1	0.44	0.029	$2.5 \cdot 10^{15}$	$4.3 \cdot 10^9$	$3.3 \cdot 10^6$
Z+2	1.07	0.0048	$2.1 \cdot 10^{14}$	$2.7 \cdot 10^{10}$	$1.8 \cdot 10^8$
Z-1	0.35	0.023	$2.0 \cdot 10^{15}$	$1.7 \cdot 10^9$	$1.3 \cdot 10^6$
Z-2	1.28	0.0074	$4.6 \cdot 10^{14}$	$2.3 \cdot 10^{10}$	$1.5 \cdot 10^8$
Z01	0.08	0.019	$1.6 \cdot 10^{15}$	$1.5 \cdot 10^9$	$1.6 \cdot 10^7$
Z02	0.58	0.0059	$3.7 \cdot 10^{14}$	$2.1 \cdot 10^{10}$	$2.1 \cdot 10^8$

B. Measurements of absorbance spectra without IS and with IS

The standard measurements of Abs spectra without IS were conducted with the single beam UV-Vis spectrophotometer Unico SQ2800. For measurements with IS, the double beam UV-Vis spectrophotometer Shimadzu-2450 was used (with ISR-3100 IS Attachment).

According to Fig. 1, one can write the following relations for light intensities and values of absorbance without and with sphere:
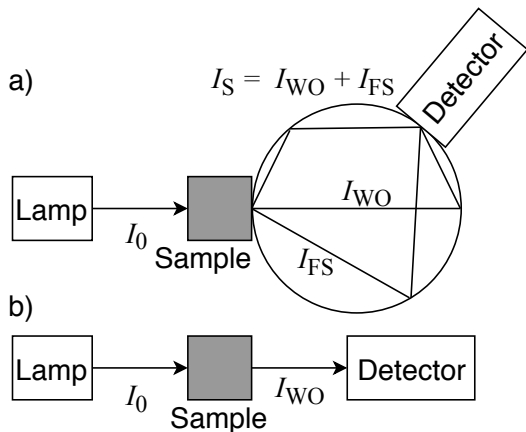
FIG. 1. Absorbance spectra measurements on a) spectrophotometer equipped with IS and b) the spectrophotometer without sphere (conventional Abs measurements). For the experiment without sphere, the forward scattered light vanishes, whereas the sphere collects it and brings the additional intensity I_{FS} into account.

$$I_{WO}(\lambda) = I_0(\lambda) \cdot 10^{-\text{Abs}_{WO}(\lambda)}, \quad (1)$$

$$I_S(\lambda) = I_{WO}(\lambda) + I_{FS}(\lambda) = I_0(\lambda) \cdot 10^{-\text{Abs}_S(\lambda)}, \quad (2)$$

where $\text{Abs}_{WO}(\lambda)$ and $\text{Abs}_S(\lambda)$ are the Abs spectra measured without and with the sphere, respectively, $I_0(\lambda)$ is the intensity of the incident beam, $I_{WO}(\lambda)$ and $I_S(\lambda)$ are the intensities after the sample, measured without and with IS respectively. $I_S(\lambda)$ is the total light intensity collected by the sphere and $I_{FS}(\lambda)$ is the intensity of light gone out from the cuvette to the sphere in the direction other than the incident beam axis corresponding to the Forward Scattered light. To be more precise, $I_0(\lambda)$ is rather an apparatus function (combination of lamp intensity and detector sensitivity), depending on the wave length. The designation (λ) after some quantities emphasizes that they have a wavelength dependence.

To compare the Abs measurements with the 90 angle scattering experiment described below, let us introduce the light scattering effectiveness as:

$$T_{FS}(\lambda) = \frac{I_{FS}(\lambda)}{I_0(\lambda)} \quad (3)$$

It is denoted with T because it is defined similar to the transmission coefficient. So, $T_{FS}(\lambda)$ has the meaning of a light fraction gone out of the cuvette away from the main optical axis and collected by the IS. From Eqs. (1) and (2) one obtains $T_{FS}(\lambda)$ as:

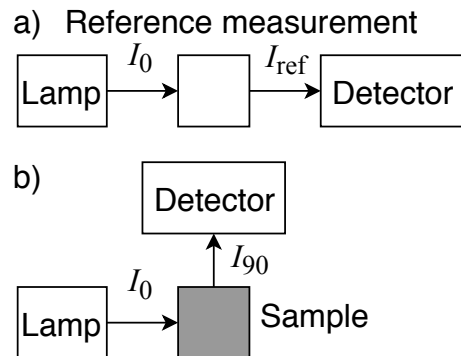$$T_{FS}(\lambda) = \left(10^{-\text{Abs}_S(\lambda)} - 10^{-\text{Abs}_{WO}(\lambda)}\right), \quad (4)$$

FIG. 2. 90 degree scattering experiment on Chirascan device giving $T_{90}(\lambda)$. Reference measurement was carried out with water in the cuvette.

C. Scattering at 90 degree angle

The Applied Photophysics Chirascan specrophotometer allows setting the photomultiplier tube detector at the angles of 0 and 90 degrees with respect to the incident light direction (see Fig. 2). At 0 degrees, the reference intensity was measured. Setting the detector at 90 degrees allowed measurements of the relative light intensity, scattered and gone out of the cuvette through its side wall. The experiment yields the 90 degree scattering in terms of effective transmission

$$T_{90}(\lambda) = \frac{I_{90}(\lambda)}{I_{ref}(\lambda)} \quad (5)$$

Both $T_{FS}(\lambda)$ and $T_{90}(\lambda)$ are generally proportional to the scattering in the hydrosol. The difference is in the scattering direction and in the detector solid angle. These quantities can be plotted in the same figure for comparison.

III. THEORY AND SIMULATION

To deeper understand the roles of absorption and scattering and separate their contributions to the nanodiamond hydrosols Abs spectra at a qualitative level, a simulation of the photon random walk in the cuvette was performed. This simulation allows establishing the interconnection between the scattering and the absorption cross sections, the DND concentrations, the Abs spectra without and with the IS, and the intensity of scattering at 90 degrees.

A. Size distribution, dielectric permittivity, and fractal structure of nanodiamonds

Here, we describe how the cross sections and the scattering indicatrices were obtained for the simulations. We have used the trimodal size distribution for nanoparticles in the hydrosol (three typical sizes of the diamond

nanoparticles) lying in agreement with the results of DLS measurements (see Figs. 3 and S1).

First, the primary crystallites of the size $D_P = 4$ nm with the particles per volume concentration n_P exist in the hydrosol. Then, we consider the medium agglomerates of the size $D_1 = 90$ nm and concentration n_1. The third type of nanoparticles is the large agglomerates of the size $D_2 = 700$ nm (concentration n_2). The adopted size of the primary nanodiamond crystallites $D_P = 4$ nm is reported in numerous papers on the detonation nanodiamonds structural properties[45-50]. The fraction of 4 nm nanodiamonds is hardly visible in the DLS data because the scattering cross section is proportional to the sixth power of nanoparticle size. Only centrifugation in very hard conditions can make the scattering from single diamond nanoparticles dominant[51].

The dielectric permittivity of the primary crystallites was taken in the form

$$\varepsilon_P(\lambda) = 5.7 + (\lambda/\lambda_0)^{-3} + iA_P \cdot (\lambda/\lambda_0)^{P_P}, \quad (6)$$

where $\lambda_0 = 300$ nm was chosen for natural normalization and $A_P = 0.17$, and $P_P = -3$ are the adjustment parameters (these values give the best fit of the experimental data). Their values were obtained preeminently by fitting the Abs spectra of Z+1 and other supernatants, see section V for more details. The first two terms of the equation above with sufficient accuracy fit the dielectric constant of the bulk diamond, given in Fig. 1 of Ref.[52]. The value of the diamond dielectric constant is also given in Ref.[53]. The third term gives the imaginary part that is essential for absorption.

The dielectric permittivity of the agglomerates does not match with one of the primary crystallites because they have a sparse fractal-like structure and contain the extensive voids filled with the medium (water). We have used the following mixing rule for calculating the agglomerate fractal dimension:

$$\varepsilon_A(D, \lambda) = \varepsilon_{A0}(\lambda) \cdot F(D) + \varepsilon_W \cdot (1 - F(D)) \quad (7)$$

where $F(D)$ is the filling factor, ε_W is the dielectric constant of water, and

$$\varepsilon_{A0}(\lambda) = 5.7 + (\lambda/\lambda_0)^{-3} + iA_A \cdot (\lambda/\lambda_0)^{P_A}, \quad (8)$$

where $A_A = 0.4$ and $P_A = -1$. The detailed analysis of calculating dielectric functions of mixtures is given in Refs.[54,55].

The filling factor can be obtained on the basis of the agglomerate size D and the size of a primary crystallite D_P via the formula[56]:

$$F(D) = C_F(D/D_P)^{3-D_f}, \quad (9)$$

where D_f is the fractal dimension of agglomerates. The used fractal dimension $D_f = 2.45$ coincides with the neutron scattering data on the spatial structure of the DND

agglomerates listed in Table 1. in Ref.[57]. $C_F = 1.9$ was an adjustment parameter. See also Ref.[58] for the data on DND fractal structure. While these studies give the fractal dimension only for the agglomerates of the size of approximately 100 nm, the self similarity allows us to extend these values to the large agglomerates of the employed trimodal model.

The difference in the imaginary part of the dielectric permittivity for the primary crystallites and agglomerates should not be surprising. As discussed below, the absorption (defined by the imaginary part of ε) in the primary particles and in the agglomerates can take place in the carbon phases of various nature. Moreover, Refs.[42,43,52,59] show that the dielectric properties of various carbon allotrope forms differ dramatically and thus some arbitrariness in the choice of ε is allowed.

The total diamond mass fraction in the hydrosol (WT2 column of Table 1) writes as

$$\mathrm{WT2} = \frac{1}{8}\frac{4\pi\rho_D}{3\rho_W}\left(n_P D_P^3 + n_1 F(D_1)D_1^3 + n_2 F(D_2)D_2^3\right) \quad (10)$$

B. Theory of light extinction in nanodiamond hydrosols

The Mie theory[60-62] was used to obtain the absorption and scattering cross sections. The calculations performed in the WOLFRAM MATHEMATICA package[63] code exaclty reproduce the results of the Matzler MATLAB code[64].

The absorption and scattering cross sections of the primary crystallites are $\sigma_P^{(\mathrm{abs})}(\lambda)$ and $\sigma_P^{(\mathrm{sca})}(\lambda)$, respectively. The input parameters for the Mie theory were the size D_P, nanoparticle dielectric permittivity $\varepsilon_P(\lambda)$, medium dielectric permittivity ε_W and wavelength λ. For the medium agglomerates, the input parameters for the Mie theory were the size $D_1 = 90$ nm, dielectric permittivity $\varepsilon_A(D_1, \lambda)$, mean dielectric permittivity ε_W, and the wavelength λ. The yield is the absorption and scattering cross sections $\sigma_1^{(\mathrm{abs})}(\lambda)$ and $\sigma_1^{(\mathrm{sca})}(\lambda)$, respectively. For the large agglomerates, the input parameters were $D_2 = 700$ nm, $\varepsilon_A(D_2, \lambda)$, ε_W and λ, and the yield was $\sigma_2^{(\mathrm{abs})}(\lambda)$ and $\sigma_2^{(\mathrm{sca})}(\lambda)$. The Mie theory also gives the scattering indicatrix used in the next section. The example of such indicatrices is plotted in Fig. S2.

The attenuation coefficient in the hydrosol due to the scattering can be written as

$$A^{(\mathrm{sca})}(\lambda) = n_1\sigma_1^{(\mathrm{sca})}(\lambda) + n_2\sigma_2^{(\mathrm{sca})}(\lambda), \quad (11)$$

and the attenuation coefficient due to absorption can be written as

$$A^{(\mathrm{abs})}(\lambda) = n_P \cdot \sigma_P^{(\mathrm{abs})}(\lambda) + n_1 \cdot \sigma_1^{(\mathrm{abs})}(\lambda) + n_2 \cdot \sigma_2^{(\mathrm{abs})}(\lambda). \quad (12)$$

Finally, the conventional absorbance (or total extinction) of the hydrosol can be written using the attenuation coefficients given by Eqs. (11) and (12):

$$\text{Abs}_{\text{WO}}(\lambda) = \frac{A^{(\text{sca})}(\lambda) \cdot L + A^{(\text{abs})}(\lambda) \cdot L}{\ln 10}, \qquad (13)$$

where L is the optical path in the cuvette.

The described model provides the best balance between the amount of free parameter (which should be kept as low as possible) and the quality of the fit of the experimental data. Using 3 different sizes is a minimal model for the description of the optical properties of nanodiamonds. 4 nm primary crystallites are the basic nanodiamond "bricks". Agglomerates of the characteristic size 90 nm are important for relatively isotropic part of scattering, evident from the $T_{90}(\lambda)$ measurements. The presence of the ≈ 700 nm agglomerates leads to the effect of forward scattering and thus they affect the measurements with the integrating sphere.

As an alternative to Eq. (7) for deriving the agglomerates dielectric permittivity, one can use the Maxwell-Garnet formula, one of the Hashin-Shtrikman bounds or Wiener bounds, see Ref.[55]. However, it will not affect significantly the decomposition of total absorbance into absorption and scattering. The same is valid for varying the sizes $D_{1,2}$, fractal dimension, and C_F. The appropriate values of n_P, n_1, and n_2 can be found to reproduce Abs spectra, $T_{\text{FS}}(\lambda)$ and $T_{90}(\lambda)$.

C. Photon random walk simulation

It is impossible to interpret the spectra $\text{Abs}(\lambda)$ obtained with the IS using only Eqs. (11) and (12) or similar equations. The study of the light propagation in the cuvette with the hydrosol using the photon random walk approach has to be done. Accounting for the scattering indicatrix obtained on the basis of Mie theory is also necessary. The similar approach is also essential for theoretical interpretation of the experiments in terms of $T_{90}(\lambda)$.

Figures S3 and S4 present the geometry of simulations. During the simulation, the photon starts in the center of the left wall of the cuvette. The propagation direction is along the optical axis (normal to the left cuvette wall). With the probability $n_1 \sigma_1^{(\text{sca})}(\lambda)$, the photon is scattered by the medium agglomerates and changes its propagation direction according to the scattering indicatrix calculated with the Mie theory. The same is for large agglomerates (index 2). The indicatrices are given in the supplementary materials[65]. Has the photon been scattered or not, it is moved by dl along its actual propagation direction. Also, at each step the photon can be absorbed with a probability $A^{(\text{abs})}(\lambda)dl$. In this case the simulation stops and goes to the next photon. The total amount of photons simulated for each wavelength was $N_{\text{total}} = 10^5$. If the photon reaches the cuvette wall, the simulation stops and also goes to the next photon.

Some areas at the walls correspond to detectors. So at the side wall (parallel to the optical axis) there was a "Chirascan detector" area of the size 0.64 cm. Taking an amount of photons fallen onto the "Chirascan detector" areas N_{90}, one can write $T_{90} = \alpha N_{90}/N_{\text{total}}$, where α was an adjustment parameter related with the actual solid angle of the detector.

The simulation allows to obtain $\text{Abs}_S(\lambda)$ as $-\log_{10}(N_S/N_{\text{total}})$, where N_S is amount of photons fallen at the right side (the side opposite to the entrance point). The conventional absorbance was obtained as $-\log_{10}(N_{\text{forw}}/N_{\text{total}})$, where N_{forw} is the amount of photons fallen onto a "normal detector" area, opposite to the entrance point. The forward scattering efficiency is $T_{\text{FS}}(\lambda) = (N_S - N_{\text{forw}})/N_{\text{total}}$.

It is important to note that the Abs spectra can be either calculated analytically using Eq. (13) or obtained with photon random walk simulation. The results of analytical calculations and photon random walk simulations coincide with sufficient accuracy (see the supplementary[65], Fig S5). In Figs. 6, S6, and S9, we plot the Abs spectra using the random walk simulations.

IV. RESULTS

A. Experimental results

The results of the size measurements for supernatants and precipitates of all samples obtained with DLS are shown in Figs. 3 and Fig. S1 in the supplementary data[65]. Fig. 4 shows the Abs spectra of all samples measured without and with IS. Fig. 5 shows the scattering efficiency in terms of $T_{\text{FS}}(\lambda)$ obtained from the Abs spectra measurements using Eq. (4) and $T_{90}(\lambda)$ from the 90 degree scattering experiment on Chirascan.
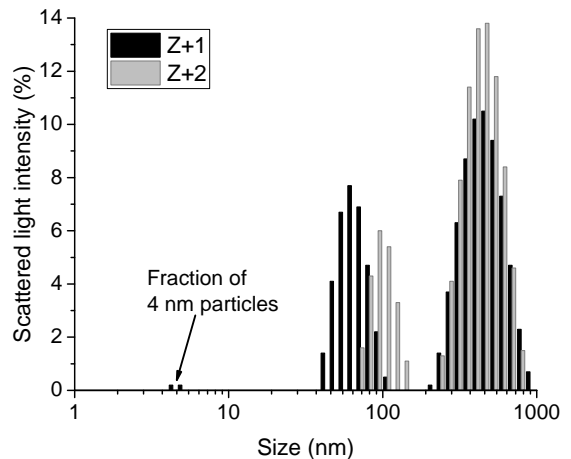

FIG. 3. Distribution by scattered light intensity for Z+ nanodiamond supernatant (Z+1) and precipitate (Z+2). One sees the trimodal size distribution.

One sees that for supernatant deagglomerated dia-

mond types (DND Z+1, Z-1), the Abs spectra without and with IS nearly coincide. It means that the scattered light intensity I_{FS} is small and the main contribution arises from the absorption. On the contrary, for all precipitates (samples Z+2, Z-2, Z02) the difference with and without the sphere is significant. The difference is also tangible for the Z01 sample, because it lacks the deagglomeration procedure and intensively scattering agglomerates remain in the hydrosol. Thus, the centrifugation process leads to separation and manifestation (due to absorption) of fraction smaller than 100 nm.

The spectra of $T_{FS}(\lambda)$ ans $T_{90}(\lambda)$ correlate with the Abs spectra without and with the sphere. Again, the scattering (both forward $T_{FS}(\lambda)$ and at 90 degree angle $T_{90}(\lambda)$) from the supernatants (the samples with the index 1) is very low and the scattering from the precipitates (the samples with the index 2) is at least one order higher. Z01 exhibits an intermediate case.
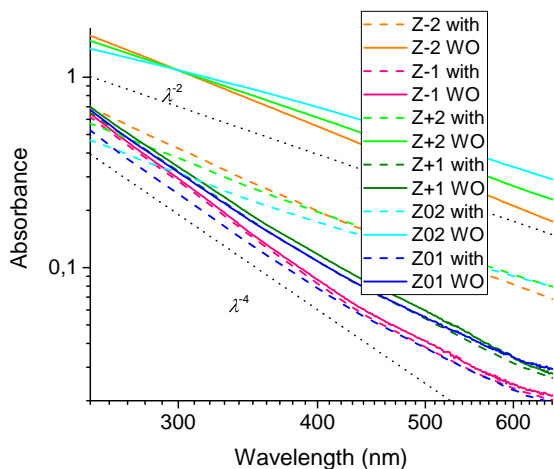

FIG. 4. Absorbance spectra for all the studied samples. Orange is for Z-2, pink is for Z-1 sample, light green is for Z+2, dark green is for Z+1, cyan is for Z02, and blue is for Z01. Solid curves are for Abs measurements without IS and dashed curves are for measurements with IS. Also, the λ^{-2} and λ^{-4} functions are plotted with dotted black curves.

Above 600 nm, the signal (and especially scattering) from the supernatants becomes too weak and comparable with the device sensitivity for both used VU-vis spectrophotometers and Chirascan.

The described analysis of Abs spectra without and with IS and the scattering efficiency ($T_{FS}(\lambda)$ and $T_{90}(\lambda)$) provides the possibility to estimate the contributions of absorption and scattering to the light extinction in nanodiamond hydrosols only qualitatively. The same data accompanied with the theory and random walk simulations allow more precise quantitative approach for the separation of absorption and scattering contributions. Additional information can be obtained on the nanoparticle size, the agglomerates fraction, and the dielectric properties of primary crystallites and agglomerates.
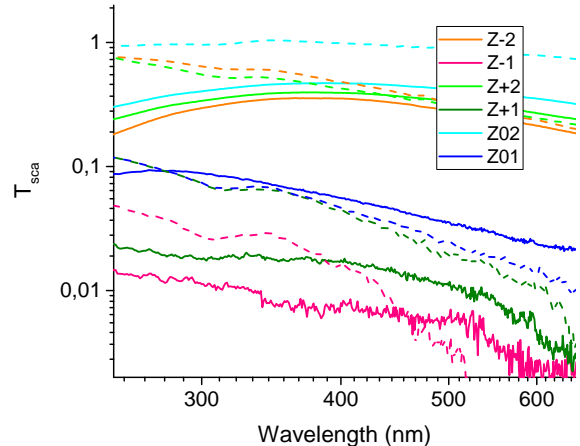

FIG. 5. Scattering effectiveness for all samples in terms of $T_{FS}(\lambda)$ and $T_{90}(\lambda)$. Solid curves are for $T_{FS}(\lambda)$ obtained from Abs measurements without and with sphere substituted to Eq. (4). Dashed curves are for 90 scattering experiment on the Chirascan device, namely $T_{90}(\lambda)$. Orange color is for Z-2 sample, pink is for Z-1 sample, light green is for Z+2, dark green is for Z+1, cyan is for Z02, and blue is for Z01.

B. Comparison of experimental data with the results of photon random walk simulation

Fig. 6 shows the $\text{Abs}_{WO}(\lambda)$ and $\text{Abs}(\lambda)$ spectra of Z+1 and Z+2 samples, calculated on the basis of photon random walks simulations with the best set of adjustment parameters compared to experimental data (see Fig. S6 and S9 for Z- ans Z0 samples, respectively). Fig. 7 shows the scattering efficiency in terms of $T_{FS}(\lambda)$ and $T_{90}(\lambda)$ (see Fig. S7 and S10 for Z- ans Z0 samples, respectively). The parameters D_f (fractal dimension), A_P, P_P, A_A, and P_A (constants in dielectric permittivity), C_F as well as the sizes D_P, D_1, and D_2 were the same for all samples (DND Z+1, Z+2, Z-1, Z-2, Z01, and Z02). For each sample n_P, n_1, and n_2 were adjusted separately.

Fig. 8 is the main result of present paper. It shows the Abs spectra decomposition into scattering and absorption contributions. Namely, Fig. 8 shows the Abs spectra of absorption and scattering obtained using Eqs. (12) and (11), respectively for Z+1 and Z+2 samples. The concentrations were adjusted and the cross sections were obtained by the Mie approach as described below. The figures plotting the similar decomposition for Z- and Z0 samples are given in supplementary (Figs. S8 and S11, respectively).
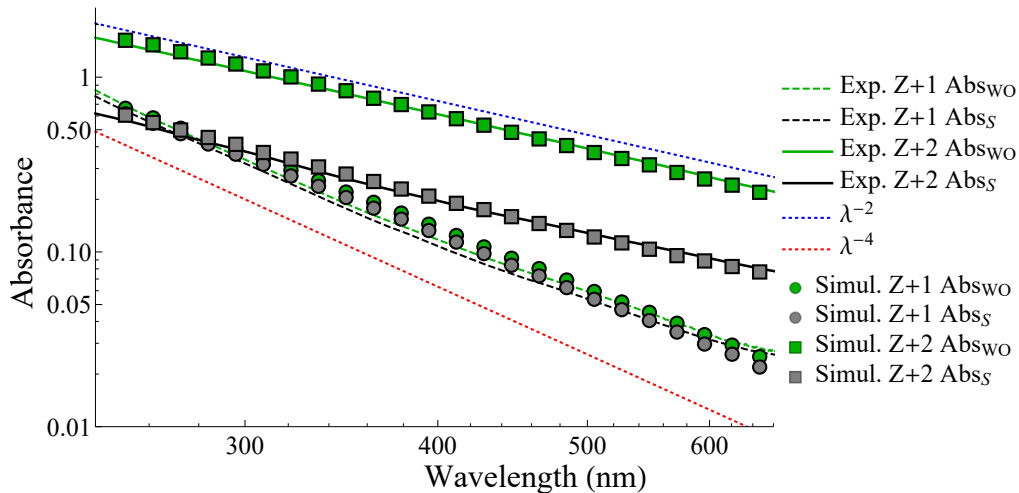
FIG. 6. The Abs spectra with and without sphere (depicted with markers), obtained with photon random walk simulation, and the experimentally measured Abs spectra of Z+1 (dashed curves) and Z+2 (solid curves) samples with (black curves) and without the sphere (green curves). The red dashed curve shows the λ^{-4} function corresponding to Rayleigh scattering and the blue dashed is for λ^{-2}.
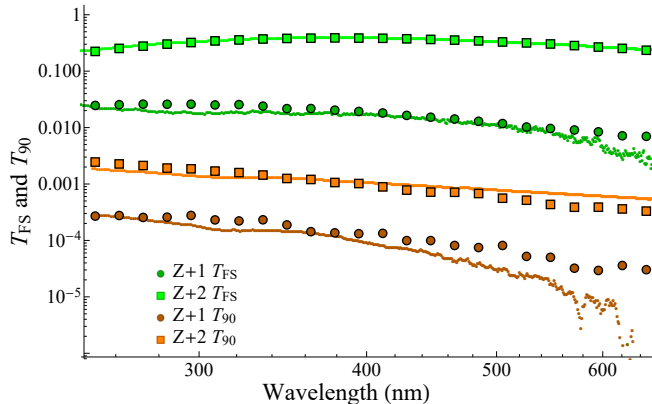

FIG. 7. The results of photon random walk simulations for scattering efficiency in terms of $T_{\mathrm{FS}}(\lambda)$ (green colors) and $T_{90}(\lambda)$ (orange colors) are shown with markers. Circles are for Z+1 and squares are for Z+2 sample. The experimental spectra are given by dense points. Experimental $T_{\mathrm{FS}}(\lambda)$ spectra were obtained on the basis of Abs measurements with and without sphere using Eq. (4) and experimental $T_{90}(\lambda)$ spectra were obtained from 90 degree scattering experiment on Chirascan device using Eq. (5).

V. DISCUSSION

A. Absorption and scattering contributions

One sees a good agreement between the predictions of the theory, the photon random walk simulations, and the experimental results. For the supernatant Z+1, the scattering is one order smaller than the absorption. The scattering in governed by the agglomerates remained in the hydrosol only. The absorption is predominantly due to primary crystallites (it is approximately 3 times higher

than the absorption from the agglomerates). For the precipitate Z+2, the scattering dominates and it is several times larger than the absorption. The scattering is obviously governed by the agglomerates. The absorption is also due to agglomerates (typically it is 10 times higher than the absorption from the primary crystallites). Thus, the optical properties of precipitates are completely defined by the agglomerates.

Interestingly, the absorption in the Z+1 sample and other supernatants is accidentally closer by its slope to the Rayleigh scattering (giving the famous λ^{-4} for the scattering cross section) than the true scattering in Z+2 sample and other precipitates in the Mie limit. That is the reason why previously[30,31,66] the nanodiamonds Abs spectra were treated as follows: first, λ^{-4} was subtracted from the spectra as some presumable scattering background, then the remaining signal was attributed to the absorption on amorphous or sp^2-like phase. From the present results, one sees that this algorithm is not correct for both precipitates and supernatants (and also for the suspension before centrifugation). Even for precipitates, the scattering contribution never overcomes 90%. Previously[30], the agglomerates were considered as solid objects, whereas in the present approach we account for their fractal sparse structure. Nevertheless, the conclusion that the scattering in DND hydrosols is due to the agglomerates (and not due to 4 nm fraction) given in previous works[30,31,66] stays intact. However, one sees that the scattering contribution to OD spectra is much smaller than thought previously.

A very similar picture takes place for the Z-1 and Z-2 samples. For Z01 sample (supernatant) the scattering is one order higher than for Z+1 and Z-1 samples (but it is still several times smaller than absorption). This picture agrees with the fact that Z0 diamond is an initial specie for Z+ and Z- preparation by means of annealing
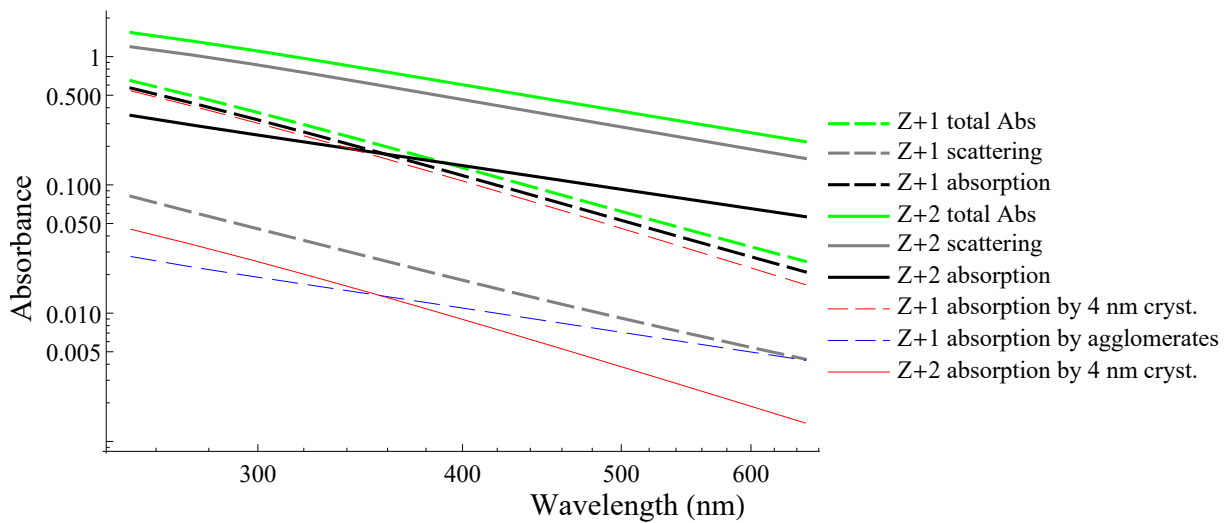
FIG. 8. Decomposition of the Abs spectra to scattering and absorption based on the Eqs (11) and (12). Solid curves are for Z+2 and dashed curves are for Z+1 samples. Green color is for total Abs, gray color is for scattering and black color is for absorption. For supernatant Z+1, the contribution to absorption from primary crystallites (red color) and agglomerates (blue color) is given. For precipitate Z+2, both scattering and absorption is governed mainly by agglomerates.

and chemical deagglomeration. According to Table I, the Z01 sample contains larger fraction of agglomerates than Z+1 and Z-1. Z02 sample is a precipitate of non deagglomerated diamond and it should contain a lot of large agglomerates. Thus, the trimodal model with the fixed sizes, suitable for all other samples, works worse for the Z02 sample. One can conclude that centrifugation is indeed a very effective way to control the optical properties of nanodiamonds[32,51,67].

From Fig. 6 one sees that the slopes of the scattering and the absorption for Z+2 sample are the same. It can be explained by the transition to the geometric optics limit caught by Mie theory. In this limit, both scattering and absorption cross sections do not depend on wavelength and they are proportional to the surface of the geometric shadow $\frac{1}{4}\pi D^2$. Importantly, the light wavelength is effectively decreased by the high value of the water refraction index, which helps to approach the limit of geometric optics. For the higher values of agglomerate size D_2 and higher fractal dimension D_f, one reaches completely the geometrical optics limit with no wavelength dependence in OD spectra (flat spectra), and an agreement of simulation and experiment can not be achieved.

From the results described above, one unambiguously concludes that the accounting for scattering in nanodiamond hydrosols absolutely requires the use of the Mie theory, because it is due to the agglomerates of the size of hundreds nanometers remaining in the solution. Due to the specific interplay between the wavelength, particle size, and dielectric properties of agglomerates (possessing the fractal structure with extensive voids), one observes the rather weird scattering slope indistinguishable from λ^{-2} for Z+2 samples. For Z-2 and Z02 the

slope is slightly different from λ^{-2}, see Figs. S6 and S9. The Rayleigh approximation is clearly not enough for the description of such structures. For 4 nm fraction, the scattering is vanishing with respect to the absorption and can be neglected. This is one of the main outcomes of the present study. The fact that the absorption always dominates or at least gives a significant contribution (dozens of percents) to absorbance, allows measuring the nanodiamond weight concentration directly, as a quantity straightly proportional to the absorbance in UV-vis range (except in the case of large agglomerates presenting specifically in precipitates).

Due to the strong absorption, the studied hydrosols are a very complicated case for investigation by the DLS technique and it can be trusted at the qualitative level only. Also, the DLS results for nanodiamond hydrosols should be necessarily supported by Abs measurements. The large D_2 agglomerates have the strongest forward scattering while the medium agglomerates (with the characteristic size of $D_1 = 90$ nm) have more isotropic scattering indicatrix. It means that the experimental data from the IS are mostly affected by larger agglomerates and for the 90 degree scattering T_{90} measured at Chirascan device, the contribution of medium agglomerates is more important.

B. Structural properties of nanodiamonds

Despite the fact that main goal of present paper was to justify that the absorption is a dominant light extinction mechanism in the nanodiamond hydrosols, one can also make some additional conclusions about the structure and the dielectric properties of nanodimonds and

their agglomerates. First, fitting the experimental data requires the assumption that the agglomerates are not solid and that they contain extensive voids. The fractal dimension 2.4 agreeing with recent SANS data[57] is consistent with the obtained experimental data.

One sees that the surface functionalization does not play a sufficient role, evident in the conducted experiments. The optical properties of all samples (Z+,Z-,Z0) can be theoretically reproduced on the basis of the same dielectric permittivity for primary particles $\varepsilon_P(\lambda)$ and agglomerates $\varepsilon_A(\lambda)$. This fact leads to the important conclusion that the absorption in the detonation nanodiamonds is an intrinsic property of a nanoparticle lattice (diamond core or reconstructed surface) and the supervenient electronic structure. We presume that the absorption is not related to the functional groups at their surface. It is known that absorption bands in the UV area in nanocarbon structures can arise from the presence of oxygen-containing moieties, for instance, the absorption feature at 300 nm in graphene oxide is commonly attributed to n-π transitions in C=O bonds of carbonyl and caboxyl groups[68]. However, the absorption spectra of DND Z+1, and DND Z-1 are almost equal, although the former one is covered with carbonhydrate moieties (CH$_2$, CH$_3$) and the latter one contains mostly carboxyls and lactones. Concluding, the absorption in DND nanoparticles can be considered to arise from electronic transitions either in the diamond core or shell. However, the exact mechanism still remains uncertain, requiring a more comprehensive study.

The agreement between experiment and theory can be achieved only if the imaginary parts of the dielectric permittivities of the agglomerates and the primary crystallites do not coincide: $A_P \neq A_A$ and $P_A \neq P_P$. This fact supports the hypothesis that the absorption takes place in the carbon phases of different nature in primary crystallites and in agglomerates. More specifically, Ref.[27] shows that sp^2 phase forms the linkages between primary DND crystallites in the agglomerates and the deagglomeration is due to removing these linkages. Thus, one can conclude that the sp^2 phase can give a dominant contribution to absorption in agglomerates. From the value of A_A and the typical magnitudes of the sp^2 and of the amorphous carbon dielectric permittivity imaginary parts, one can estimate that the fraction of the non-diamond phase for the agglomerates reaches a dozen of percents.

For the primary crystallites, the absorption can be due to the Urbach tail in the electron density of states (due to the disorder) near the band gap edge. However, this hypothesis implies the exponential wavelength dependence of ε_P imaginary part, see e.g. Ref.[43]. But we did not manage to fit Im$\{\varepsilon_P\}$ in the exponential form for explaining absorption in the DND Z+1, Z-1, and Z01 samples.

The power function with the best fit quality corresponds to $P_P = -3$. The second hypothesis explains the absorption by the amorphous shell with sp^{3-x} hybridization or graphite-like phase[29,69,70]. Fig. 2 from Ref.[59] shows the dielectric permittivities of various types of amorphous carbon differ dramatically, which allows certain arbitrariness when tuning the dielectric permittivity. E.g. approximating with the power function the dependence for ta-C in Ref.[59] one obtains $P_P \approx -2$. In the assumption that the absorption in primary diamond crystallites comes from the sp^{3-x} shell, using the adjusted value of A_P one can estimate the fraction of such phase as several percents. The latter quantity is an essential input parameter for modelling the disorder effects and line width in the nanodiamonds Raman spectra using microscopic DMM-BPM or continuous EKFG models[71,72].

VI. CONCLUSION

As a net result, it is demonstrated that the preeminent part of the individual DND particles optical spectra is governed by the absorption of light, and not by its scattering. The scattering begins to dominate only for the DND agglomerates with the lateral size of several hundreds of nanometers. Although the exact mechanism underlying the absorption process remains unclear, the obtained results give a deeper understanding of the DND optical properties and allow to clarify the calculations involved in the analysis of the DND fluorescence spectra and particle size using dynamic light scattering. Normal Abs measurements supported by the measurements with IS or by measurements of side scattering allow distinguishing the contributions of scattering and absorption to nanodiamond spectra and can provide a deeper insight into the properties of their surface and phase composition. Clarification of the absorption mechanism in the primary DND crystallites and creation of an appropriate theoretical model is a bright challenge for the future studies of nanodiamonds.

* kon@mail.ioffe.ru

[1] Y. Y. Hui, C.-L. Cheng, and H.-C. Chang, Journal of Physics D: Applied Physics **43**, 374021 (2010).

[2] D. N. Ho, Springer US) **10**, 978 (2010).

[3] A. M. Schrand, S. A. C. Hens, and O. A. Shenderova, Critical reviews in solid state and materials sciences **34**, 18 (2009).

[4] V. N. Mochalin, O. Shenderova, D. Ho, and Y. Gogotsi, Nature nanotechnology **7**, 11 (2012).

[5] J.-C. Arnault, *Nanodiamonds: Advanced Material Analysis, Properties and Applications* (William Andrew, 2017).

[6] S. Kidalov, F. Shakhov, and A. Y. Vul, Diamond and Related Materials **16**, 2063 (2007).

[7] J.-P. Boudou, P. A. Curmi, F. Jelezko, J. Wrachtrup, P. Aubert, M. Sennour, G. Balasubramanian, R. Reuter, A. Thorel, and E. Gaffet, Nanotechnology **20**, 235602 (2009).

[8] Y.-C. Chen, P. S. Salter, S. Knauer, L. Weng, A. C. Frangeskou, C. J. Stephen, S. N. Ishmael, P. R. Dolan, S. Johnson, B. L. Green, G. W. Morley, M. E. Newton, J. G. Rarity, M. J. Booth, and J. M. Smith, Nat Photon **11**, 77 (2017), letter.

[9] A. Stacey, T. Karle, L. McGuinness, B. Gibson, K. Ganesan, S. Tomljenovic-Hanic, A. Greentree, A. Hoffman, R. Beausoleil, and S. Prawer, Applied Physics Letters **100**, 071902 (2012).

[10] M. Fujiwara, R. Tsukahara, Y. Sera, H. Yukawa, Y. Baba, S. Shikata, and H. Hashimoto, arXiv preprint arXiv:1802.07431 (2018).

[11] J. Tisler, G. Balasubramanian, B. Naydenov, R. Kolesov, B. Grotz, R. Reuter, J.-P. Boudou, P. A. Curmi, M. Sennour, A. Thorel, *et al.*, ACS nano **3**, 1959 (2009).

[12] P. Neumann, N. Mizuochi, F. Rempp, P. Hemmer, H. Watanabe, S. Yamasaki, V. Jacques, T. Gaebel, F. Jelezko, and J. Wrachtrup, Science **320**, 1326 (2008).

[13] L. Robledo, L. Childress, H. Bernien, B. Hensen, P. F. Alkemade, and R. Hanson, Nature **477**, 574 (2011).

[14] H. Bernien, L. Childress, L. Robledo, M. Markham, D. Twitchen, and R. Hanson, Physical Review Letters **108**, 043604 (2012).

[15] K. D. Behler, A. Stravato, V. Mochalin, G. Korneva, G. Yushin, and Y. Gogotsi, ACS nano **3**, 363 (2009).

[16] U. Maitra, K. E. Prasad, U. Ramamurty, and C. Rao, Solid State Communications **149**, 1693 (2009).

[17] X. Chen, B. Zhang, Y. Gong, P. Zhou, and H. Li, Applied Surface Science **439**, 60 (2018).

[18] O. Faklaris, V. Joshi, T. Irinopoulou, P. Tauc, M. Sennour, H. Girard, C. Gesset, J.-C. Arnault, A. Thorel, J.-P. Boudou, *et al.*, ACS nano **3**, 3955 (2009).

[19] N. Nunn, M. dAmora, N. Prabhakar, A. M. Panich, N. Froumin, M. D. Torelli, I. Vlasov, P. Reineck, B. Gibson, J. M. Rosenholm, *et al.*, Methods and applications in fluorescence **6**, 035010 (2018).

[20] H. Zhu, Y. Wang, A. Hussain, Z. Zhang, Y. Shen, and S. Guo, Journal of Materials Chemistry B **5**, 3531 (2017).

[21] J.-P. Boudou, J. Tisler, R. Reuter, A. Thorel, P. A. Curmi, F. Jelezko, and J. Wrachtrup, Diamond and Related Materials **37**, 80 (2013).

[22] S. Stehlik, M. Varga, M. Ledinsky, V. Jirasek, A. Artemenko, H. Kozak, L. Ondic, V. Skalova, G. Argentero, T. Pennycook, *et al.*, The Journal of Physical Chemistry C **119**, 27708 (2015).

[23] M. Baidakova, Y. A. Kukushkina, A. Sitnikova, M. Yagovkina, D. Kirilenko, V. Sokolov, M. Shestakov, A. Y. Vul, B. Zousman, and O. Levinson, Physics of the Solid State **55**, 1747 (2013).

[24] A. Shiryaev, A. Fisenko, I. Vlasov, L. Semjonova, P. Nagel, and S. Schuppler, Geochimica et Cosmochimica Acta **75**, 3155 (2011).

[25] O. Shenderova *et al.*, *Detonation nanodiamonds: science and applications* (CRC Press, 2014).

[26] S. Stehlik, M. Varga, M. Ledinsky, D. Miliaieva, H. Kozak, V. Skakalova, C. Mangler, T. J. Pennycook, J. C. Meyer, A. Kromka, *et al.*, Scientific reports **6**, 38419 (2016).

[27] A. Dideikin, A. Aleksenskii, M. Baidakova, P. Brunkov, M. Brzhezinskaya, V. Y. Davydov, V. Levitskii, S. Kidalov, Y. A. Kukushkina, D. Kirilenko, *et al.*, Carbon **122**, 737 (2017).

[28] N. Kuznetsov, S. Belousov, D. Y. Stolyarova, A. Bakirov, S. Chvalun, A. Shvidchenko, E. Eidelman, and A. Y. Vul, Diamond and Related Materials **83**, 141 (2018).

[29] S. Tomita, M. Fujii, and S. Hayashi, Physical Review B **66**, 245424 (2002).

[30] A. Y. Vul, E. Eydelman, L. Sharonova, A. Aleksenskiy, and S. Konyakhin, Diamond and Related Materials **20**, 279 (2011).

[31] A. Aleksenskii, A. Y. Vul, S. Konyakhin, K. Reich, L. Sharonova, and E. Eidelman, Physics of the Solid State **54**, 578 (2012).

[32] L. Usoltseva, D. Volkov, D. Nedosekin, M. Korobov, M. Proskurnin, and V. Zharov, Photoacoustics (2018).

[33] D. Volkov, P. Semenyuk, M. Korobov, and M. Proskurnin, Journal of analytical chemistry **67**, 842 (2012).

[34] E. Osawa, NCRI Technical Bulletin **2**, 1365 (2007).

[35] E. Ōsawa, Pure and Applied Chemistry **80**, 1365 (2008).

[36] S. Koniakhin, I. Eliseev, I. Terterov, A. Shvidchenko, E. Eidelman, and M. Dubina, Microfluidics and Nanofluidics **18**, 1189 (2015).

[37] A. Aleksenskii, A. Shvidchenko, and E. Eidelman, Technical Physics Letters **38**, 1049 (2012).

[38] M. Hauf, B. Grotz, B. Naydenov, M. Dankerl, S. Pezzagna, J. Meijer, F. Jelezko, J. Wrachtrup, M. Stutzmann, F. Reinhard, *et al.*, Physical Review B **83**, 081304 (2011).

[39] B. Ofori-Okai, S. Pezzagna, K. Chang, M. Loretz, R. Schirhagl, Y. Tao, B. Moores, K. Groot-Berning, J. Meijer, and C. Degen, Physical Review B **86**, 081406 (2012).

[40] M. Loretz, S. Pezzagna, J. Meijer, and C. Degen, Applied Physics Letters **104**, 033102 (2014).

[41] A. A. Lucas, L. Henrard, and P. Lambin, Phys. Rev. B **49**, 2888 (1994).

[42] B. Draine and H. M. Lee, The Astrophysical Journal **285**, 89 (1984).

[43] G. Vantarakis, C. Mathioudakis, G. Kopidakis, C. Wang, K. Ho, and P. Kelires, Physical Review B **80**, 045307 (2009).

[44] L. Schmidlin, V. Pichot, M. Comet, S. Josset, P. Rabu, and D. Spitzer, Diamond and Related Materials **22**, 113 (2012).

[45] S. Osswald, V. Mochalin, M. Havel, G. Yushin, and Y. Gogotsi, Physical Review B **80**, 075419 (2009).

[46] A. Y. Vul, A. Dideikin, Z. Tsareva, M. Korytov, P. Brunkov, B. Zhukov, and S. Rozov, Technical physics letters **32**, 561 (2006).

[47] A. Aleksenskii, M. Baidakova, A. Y. Vul, V. Y. Davydov, and Y. A. Pevtsova, Physics of the Solid State **39**, 1007 (1997).

[48] A. Aleksenskii, M. Baidakova, A. Y. Vul, and V. Siklitskii, Physics of the Solid State **41**, 668 (1999).

[49] O. A. Shenderova, I. I. Vlasov, S. Turner, G. Van Tendeloo, S. B. Orlinskii, A. A. Shiryaev, A. A. Khomich, S. N.

Sulyanov, F. Jelezko, and J. Wrachtrup, The Journal of Physical Chemistry C **115**, 14014 (2011).

[50] A. Ozerin, T. Kurkin, L. Ozerina, and V. Y. Dolmatov, Crystallography Reports **53**, 60 (2008).

[51] S. Koniakhin, N. Besedina, D. Kirilenko, A. Shvidchenko, and E. Eidelman, Superlattices and Microstructures **113**, 204 (2018).

[52] D. F. Edwards and E. Ochoa, JOSA **71**, 607 (1981).

[53] S. Bhagavantam and D. N. RAO, Nature **161**, 729 (1948).

[54] J. Reynolds and J. Hough, Proceedings of the Physical Society. Section B **70**, 769 (1957).

[55] K. K. Karkkainen, A. H. Sihvola, and K. I. Nikoskinen, IEEE Transactions on Geoscience and Remote Sensing **38**, 1303 (2000).

[56] C. Sorensen, Aerosol Science & Technology **35**, 648 (2001).

[57] O. V. Tomchuk, D. S. Volkov, L. A. Bulavin, A. V. Rogachev, M. A. Proskurnin, M. V. Korobov, and M. V. Avdeev, The Journal of Physical Chemistry C **119**, 794 (2014).

[58] M. Baidakova, V. Siklitsky, and A. Y. Vul, Chaos, Solitons & Fractals **10**, 2153 (1999).

[59] M. Gioti and S. Logothetidis, Diamond and related materials **12**, 957 (2003).

[60] G. Mie, Annalen der physik **330**, 377 (1908).

[61] H. C. Hulst and H. C. van de Hulst, *Light scattering by small particles* (Courier Corporation, 1957).

[62] C. F. Bohren and D. R. Huffman, *Absorption and scattering by a sphere* (Wiley Online Library, 1983).

[63] W. Mathematica, Inc., Champaign, Illinois (2009).

[64] C. Mätzler, IAP Res. Rep **8**, 1 (2002).

[65] See Supplemental Material on the arXiv.

[66] S. Konyakhin, L. Sharonova, and E. Eidelman, Technical Physics Letters **39**, 244 (2013).

[67] A. Trofimuk, D. Muravijova, D. Kirilenko, and A. Shvidchenko, Materials **11**, 1285 (2018).

[68] P. V. Kumar, N. M. Bardhan, S. Tongay, J. Wu, A. M. Belcher, and J. C. Grossman, Nature chemistry **6**, 151 (2014).

[69] V. I. Korepanov, H.-o. Hamaguchi, E. Osawa, V. Ermolenkov, I. K. Lednev, B. J. Etzold, O. Levinson, B. Zousman, C. P. Epperla, and H.-C. Chang, Carbon **121**, 322 (2017).

[70] M. Mermoux, S. Chang, H. A. Girard, and J.-C. Arnault, Diamond and Related Materials (2018).

[71] S. V. Koniakhin, O. I. Utesov, I. N. Terterov, A. V. Siklitskaya, A. G. Yashenkin, and D. Solnyshkov, The Journal of Physical Chemistry C **122**, 19219 (2018).

[72] O. I. Utesov, A. G. Yashenkin, and S. V. Koniakhin, The Journal of Physical Chemistry C **122**, 22738 (2018).